Synthesis, characterisation and properties towards CO_2 reduction into CO of a Cr(III) diphenyl quaterpyridine complex.

Kabibi-Charles Kamashanju, Mathieu Curtil, Florian Molton, Nikolaus Vlachopoulos, Fabrice Thomas, ,Jérôme Chauvin*

Univ. Grenoble Alpes, CNRS, DCM UMR 5250, F-38000 Grenoble, France

Supporting Information

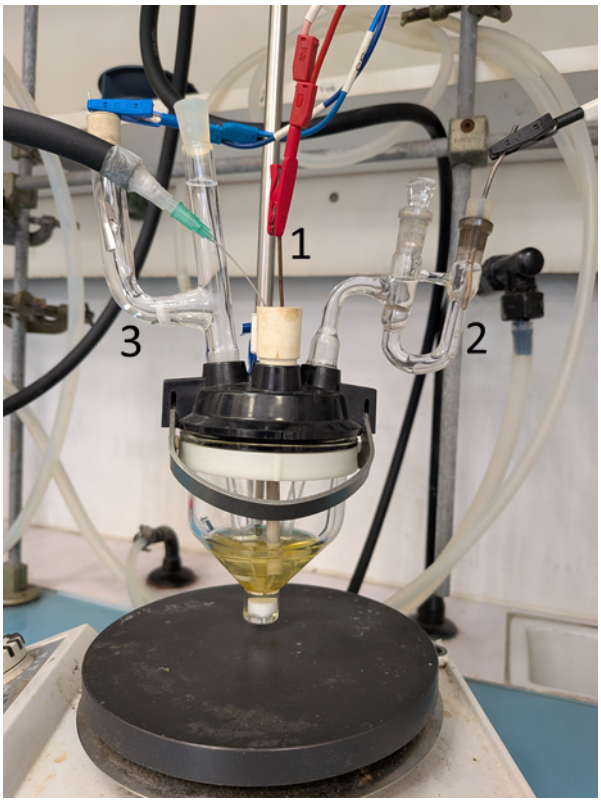

1-Figures :

Figure S1. Three electrodes cell (1: working electrode: glassy carbon (diam = 3 mm) or carbon foam (80 dpi) ; 2 : reference electrode : $Ag/AgNO_3$ 10^{-2} M in DMF + 0.1 M $TBAPF_6$; 3: auxiliary electrode : a platinum plate immersed in DMF + 0.1 M $TBAPF_6$, separated by a frit).

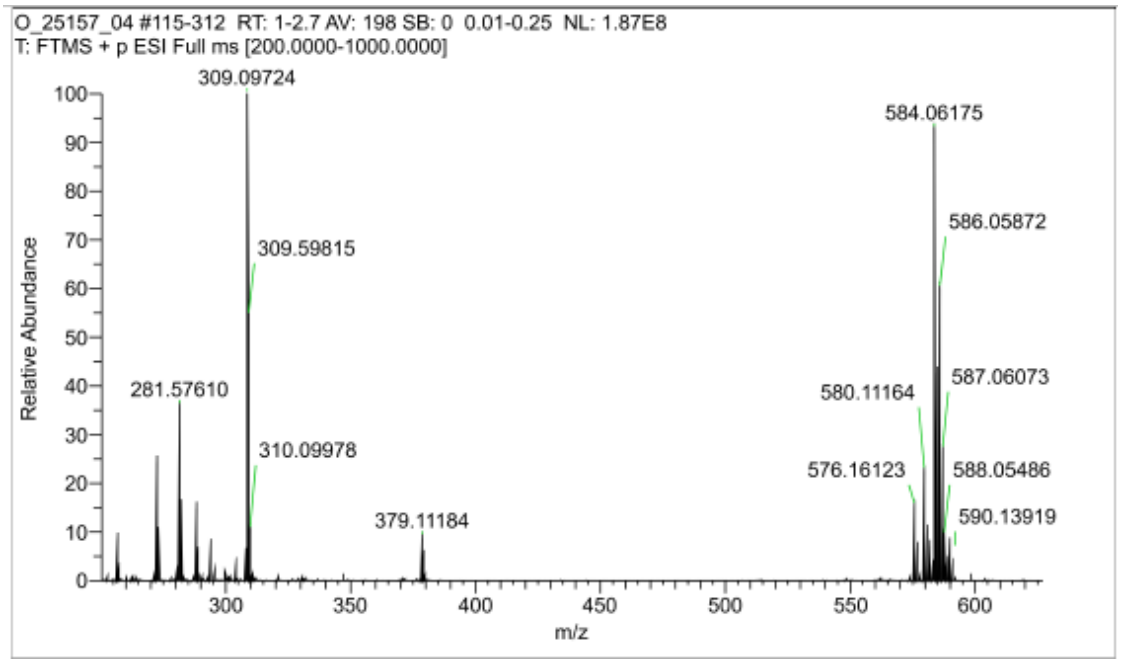

Figure S2. High Resolution Mass Spectrum of $[Cr(dpqpy)(Cl)_2]^+$

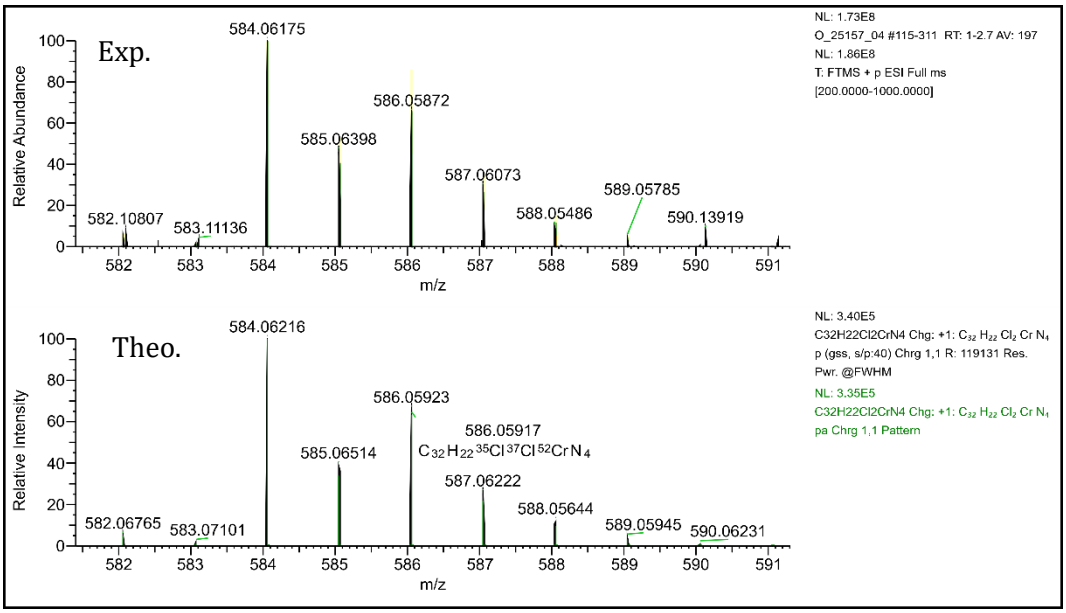

Figure S3. High Resolution Mass Spectrum of $[Cr(dpqpy)(Cl)_2]^+$: mass peak analysis.

Peak Mass	Display Formula	Delta [ppm]	Theo. mass	Pattern Cov. [%]	MSMS Matched Frag...
582.06754	$C_{32}H_{22}N_4{}^{35}Cl_2{}^{50}Cr$	-0.20	582.06765	97.46	(Collection)

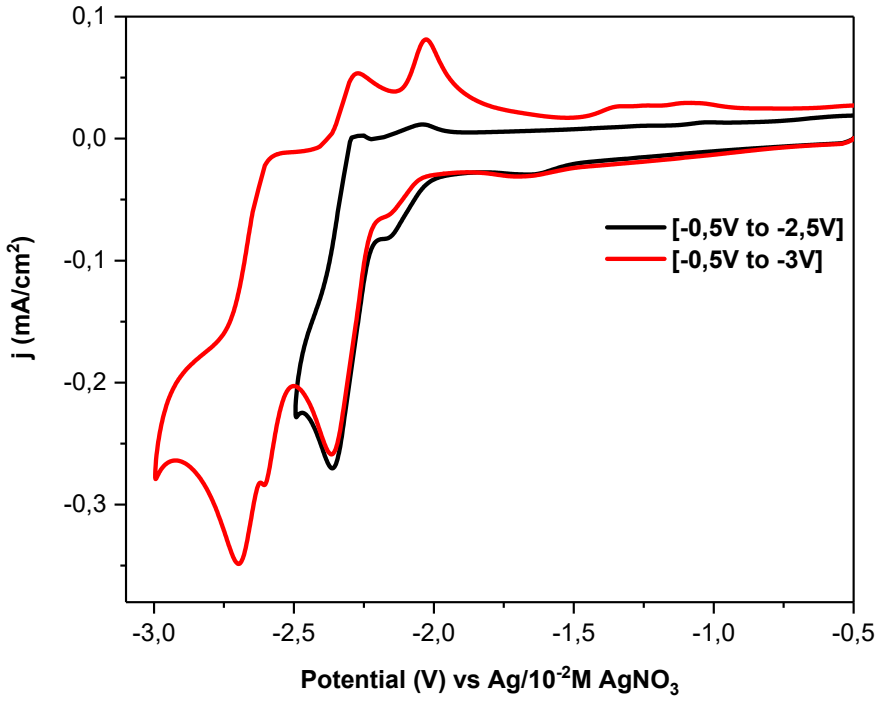

Figure S4. Cathodic cyclic voltammetry scans of a 1mM of the diphenyl quaterpyridine ligand (dpqpy) under argon atmosphere on a glassy carbon electrode (GCE) in DMF/0.1M $TBAPF_6$ at $v = 0.1Vs^{-1}$, electrode area 0.071 cm^2.

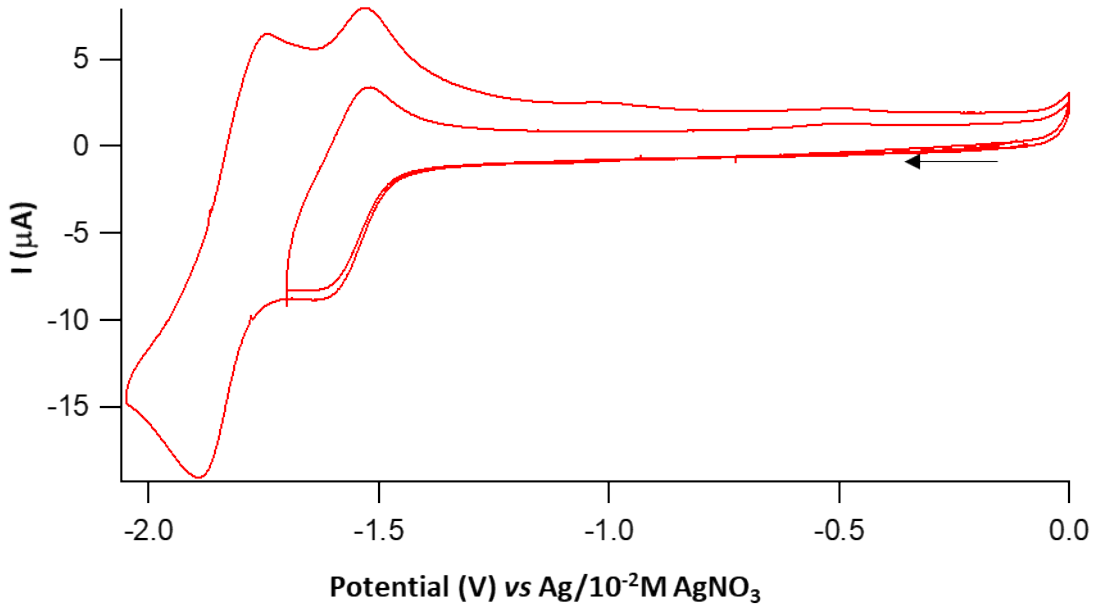

Figure S5. Cyclic voltammetry scan of 1mM [Zn(dpqpy)(Cl)$_2$] in DMF/0.1M TBAPF$_6$ performed under argon atmosphere on a GCE at v = 0.1Vs^{-1}, electrode area 0.071 cm^2.

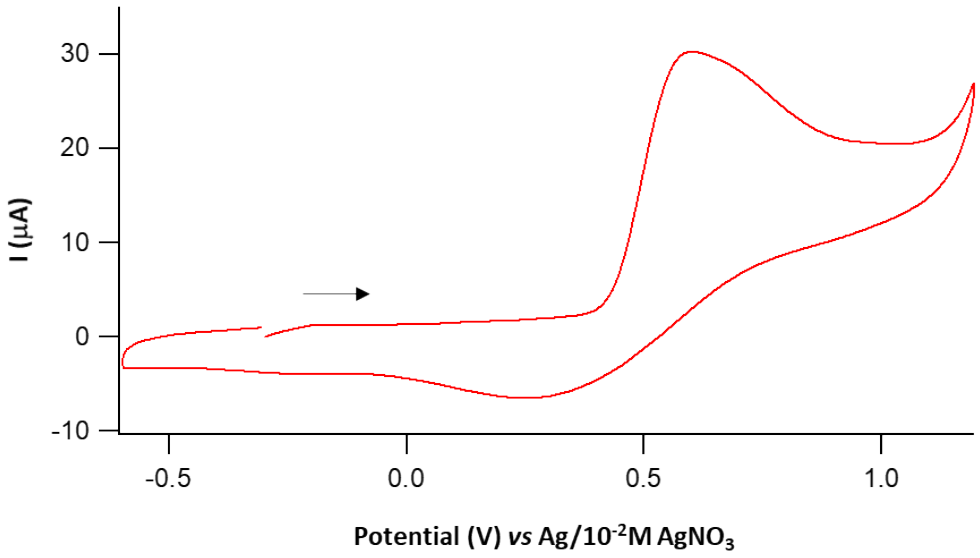

Figure S6. Cyclic voltammetry scan of 2mM [N(Et)$_4$]$^+$,Cl$^-$ in DMF/0.1M TBAPF$_6$ on a GCE at v = 0.1Vs^{-1}, electrode area 0.071 cm^2.

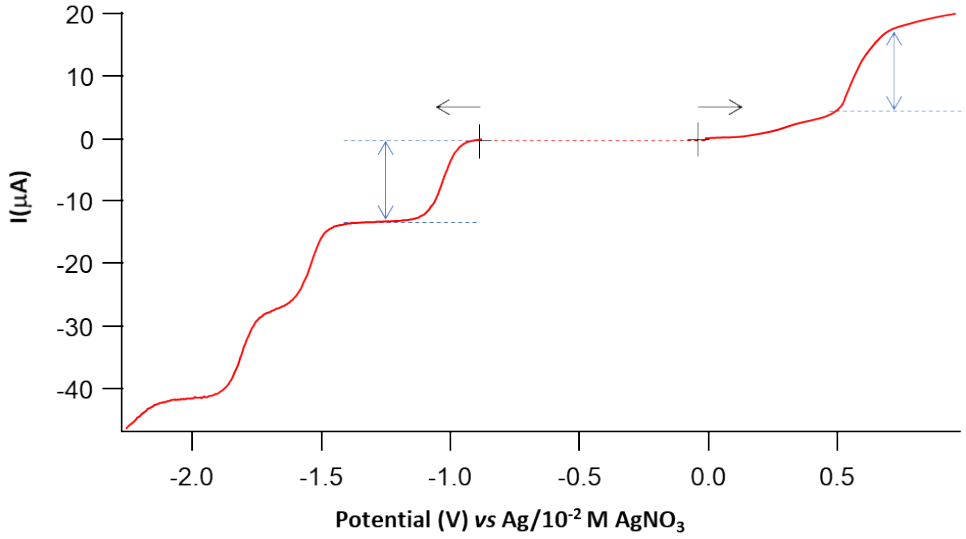

Figure S7. Rotating disk electrode experiments performed with 1mM $[Cr(dpqpy)(Cl)_2]^+$ complex in DMF/0.1M $TBAPF_6$ at 10 mV s^{-1} under argon atmosphere on a GCE (diam. 3mm, rate of rotation 200 rpm).

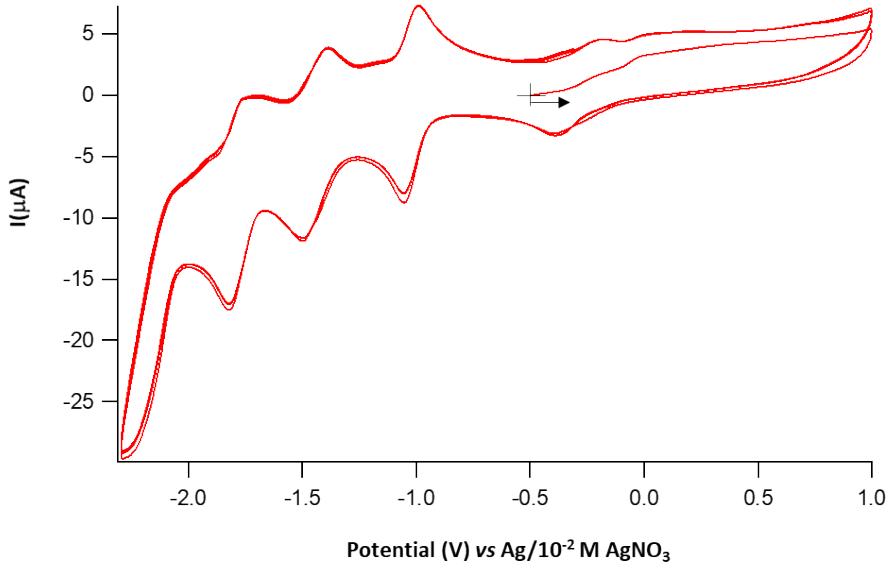

Figure S8. Cyclic voltammetry scan of 1mM $[Cr(dpqpy)(Cl)_2]^+$ in DMF/0.1M $TBAPF_6$ performed after exhaustive electrolysis of the solution performed at 0.6 V at v = 0.1Vs^{-1}, electrode area 0.071 cm^2.

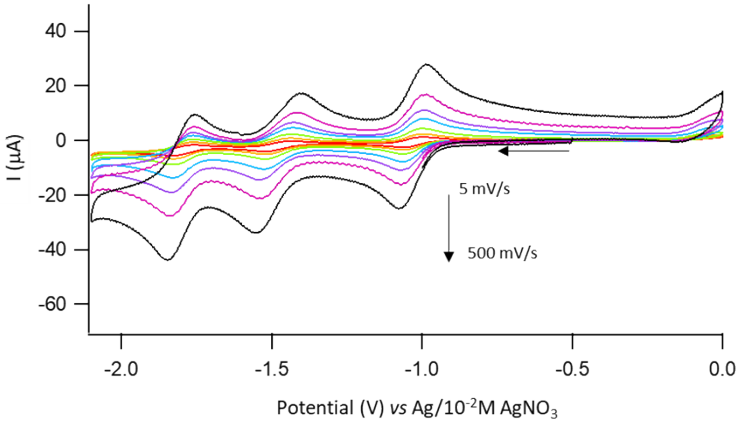

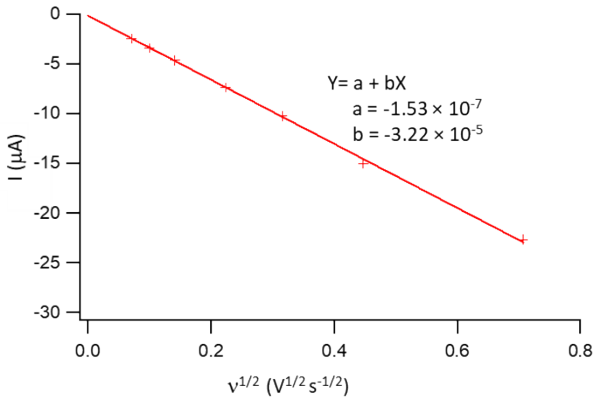

Figure S9. Left : Cyclic voltammetry scan of 1mM $[Cr(dpqpy)(Cl)_2]^+$ in DMF/0.1M $TBAPF_6$ performed at different scan rate : 5, 10, 20, 50, 100, 200 and 500 mV/s, electrode area 0.071 cm^2, T = 20°C; Right : The Randles–Ševčík plot for the first reduction wave, the diffusion coefficient of $[Cr(dpqpy)(Cl)_2]^+$ is estimated to 2.82×10^{-6} cm^2/s.

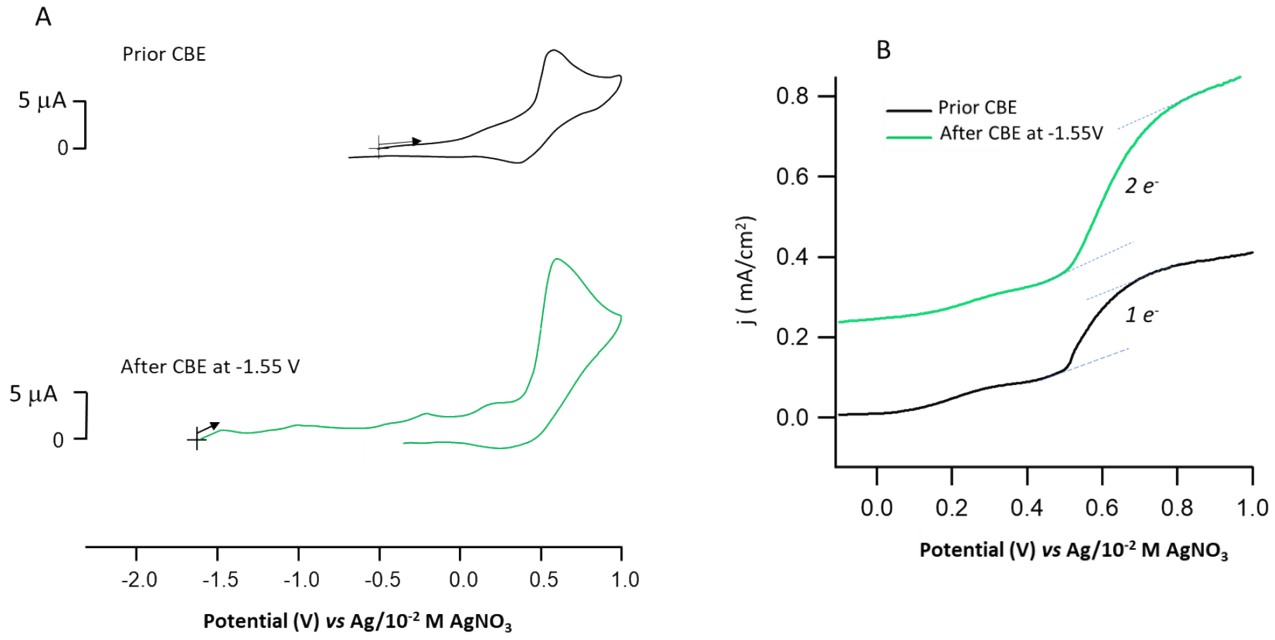

Figure S10. Cyclic voltammetry scan (A) (at $v = 0.1Vs^{-1}$, electrode area 0.071 cm^2) and rotating disk electrode experiments (B) (at $v = 0.01Vs^{-1}$, rate of rotation 200 rpm, electrode area 0.071 cm^2) performed with 1mM $[Cr(dpqpy)(Cl)_2]^+$ in DMF/0.1M $TBAPF_6$ on GCE prior and after cathodic bulk electrolysis at -1.55 V.

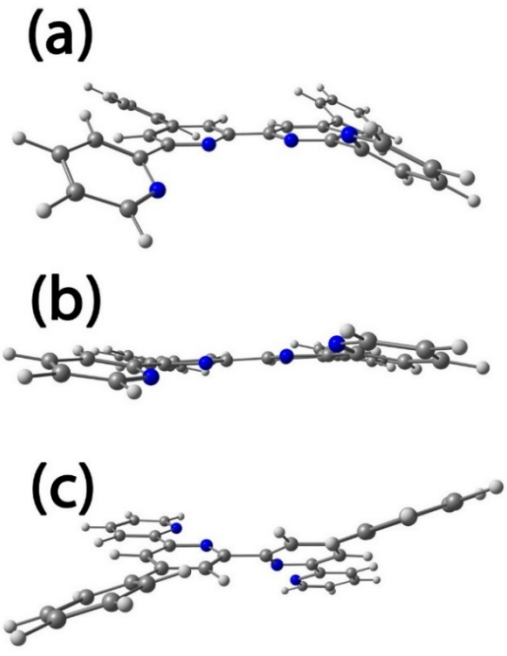

Figure S11. Geometry optimized structures of the free ligand, from a B3LYP/6-31g* calculation: a) ($dpqpy^{\bullet -}$) (doublet); b) ($dpqpy^{2-}$) (singlet); ($dpqpy^{2\bullet 2-}$) (triplet). The bipyridine core is tilted in (c), the two N atoms retaining their cis conformation.

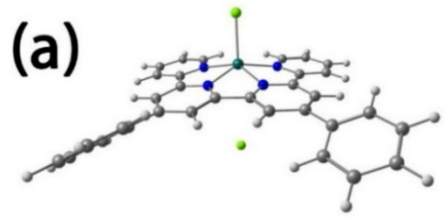

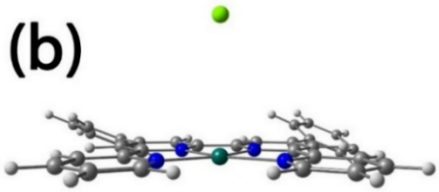

Figure S12. Geometry optimized structures of the zinc complex $[Zn(dpqpy)(Cl)_2]^{2-}$, from a B3LYP/6-31g* calculation: a) triplet; b) closed-shell singlet.

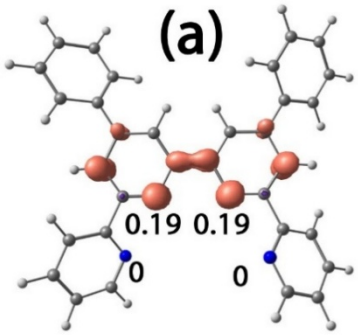

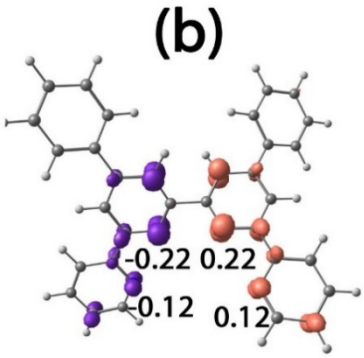

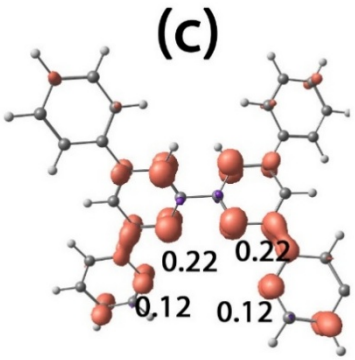

Figure S13. Spin density plot from a B3LYP/6-31g* calculation. Isosurface shown with 0.005410 contour value: a) ($dpqpy^{\bullet -}$) (doublet); b) ($dpqpy^{2\bullet 2-}$) (BS singlet); c) ($dpqpy^{2\bullet 2-}$) (triplet). The Mulliken spin population on the N atoms is indicated.

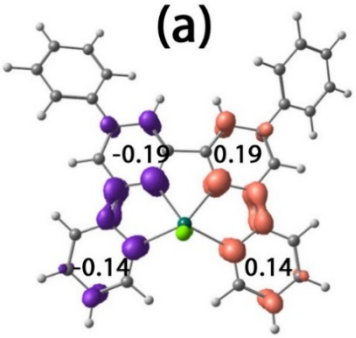

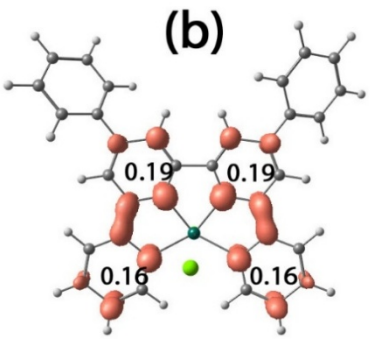

Figure S14. Spin density plot of the zinc complex $[Zn(dpqpy)(Cl)_2]^{2-}$, from a B3LYP/6-31g* calculation. Isosurface shown with 0.005410 contour value: a) BS singlet; b) triplet. The Mulliken spin population on the N atoms is indicated.

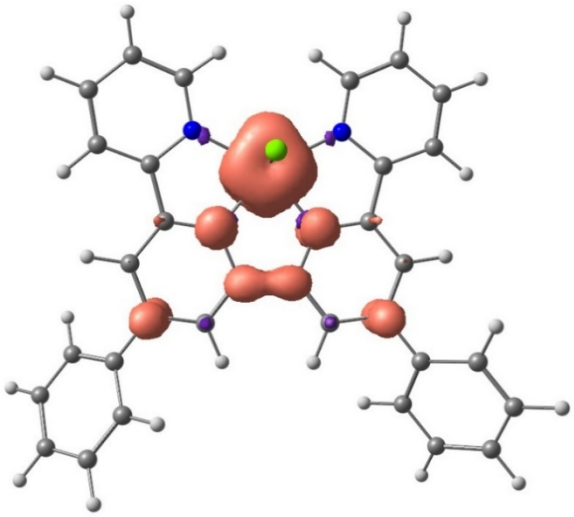

Figure S15. Spin density plot from a D3-B3LYP/6-31g*/PCM calculation. Isosurface shown with 0.005410 contour value: one-electron reduced $[Cr(dpqpy)(Cl)_2]^0$ (quintet).

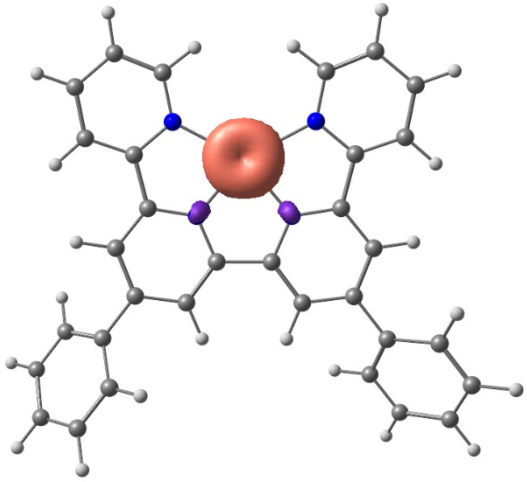

Figure S16. Spin density plot of the one-electron reduced $[Cr(dpqpy)]^{2+}$ (triplet). From a D3-B3LYP/6-31g*/PCM calculation; Isosurface shown with 0.005410 contour value.

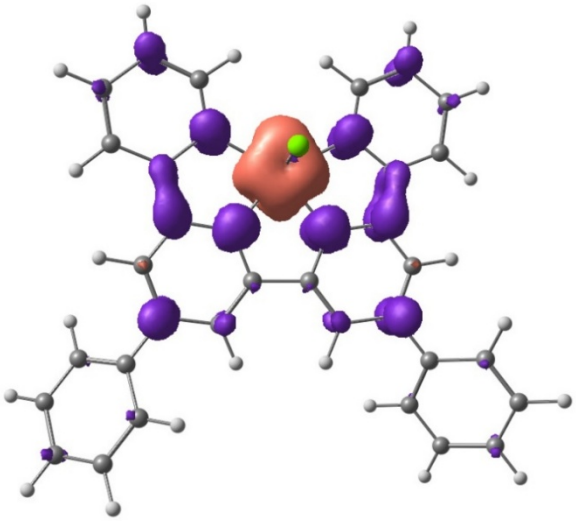

Figure S17. Spin density plot of the two-electron reduced $[Cr(dpqpy)(Cl)_2]^-$ (quartet). From a D3-B3LYP/6-31g*/PCM calculation; Isosurface shown with 0.005410 contour value.

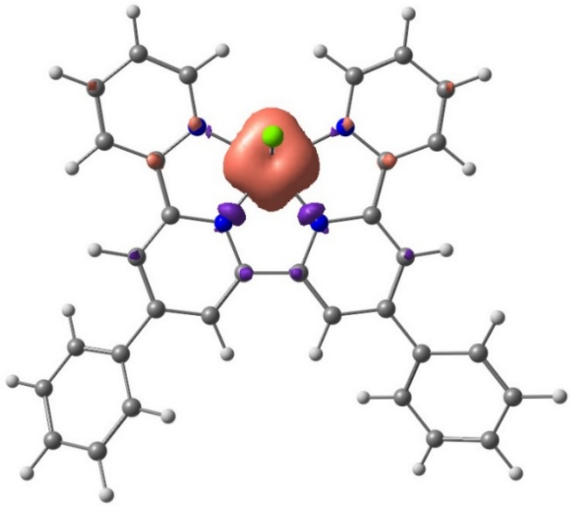

Figure S18. Spin density plot of the two-electron reduced $[Cr(dpqpy)(Cl)_2]^-$ (sextet). From a D3-B3LYP/6-31g*/PCM calculation; Isosurface shown with 0.005410 contour value.

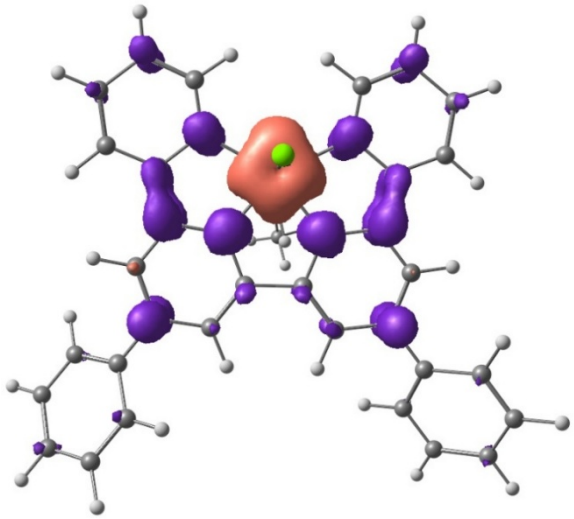

Figure S19. Spin density plot of the two-electron reduced $[Cr(dpqpy)(Cl)(DMF)]^0$ (doublet). From a D3-B3LYP/6-31g*/PCM calculation; Isosurface shown with 0.005410 contour value.

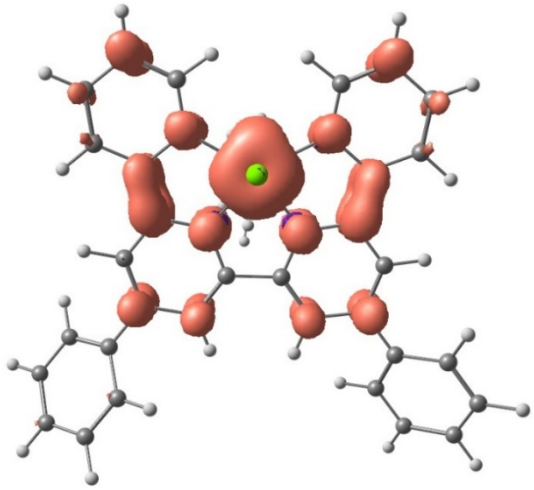

Figure S20. Spin density plot of the two-electron reduced $[Cr(dpqpy)(Cl)(DMF)]^0$ (sextet). From a D3-B3LYP/6-31g*/PCM calculation; Isosurface shown with 0.005410 contour value.

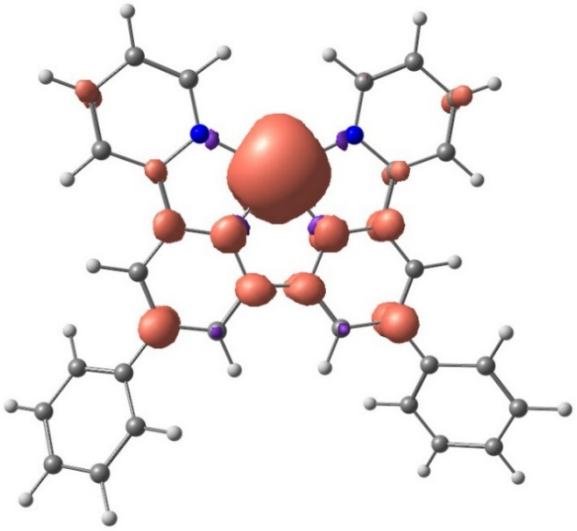

Figure S21. Spin density plot of the two-electron reduced $[Cr(dpqpy)]^+$ (sextet). From a D3-B3LYP/6-31g*/PCM calculation; Isosurface shown with 0.005410 contour value.

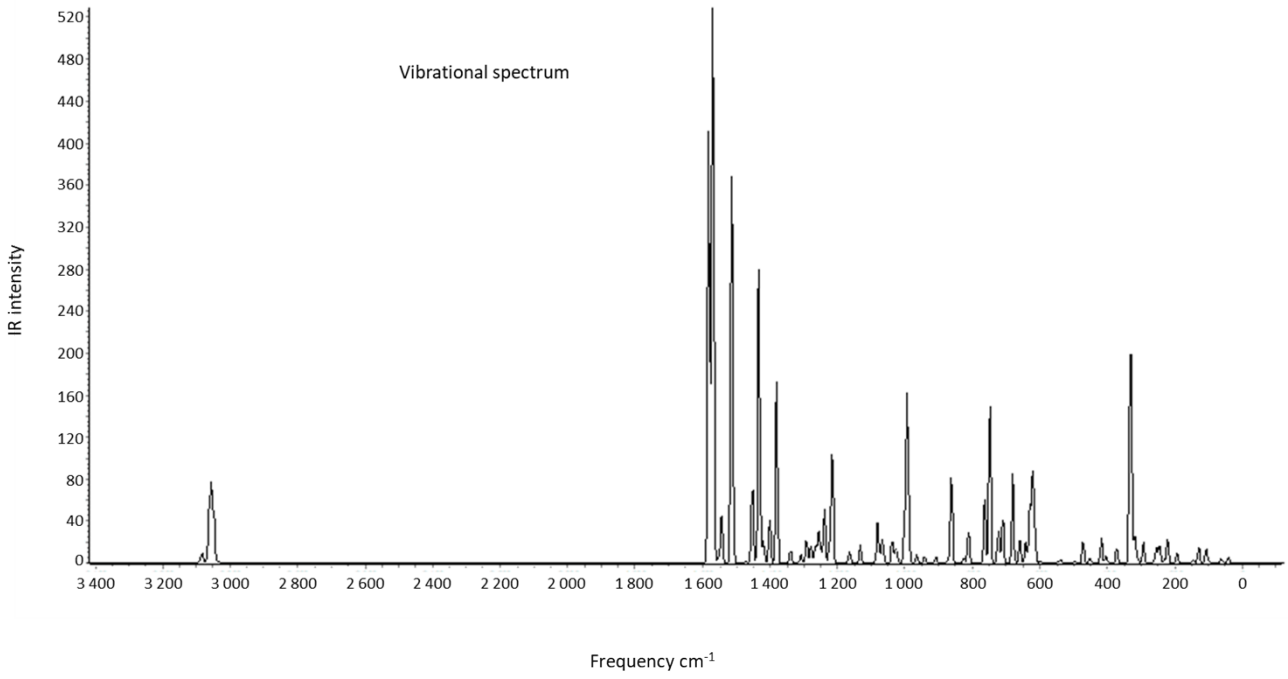

Figure S22. Calculated vibrational spectrum of $[Cr(dpqpy)(Cl)_2]^+$, with scaled frequencies. Methodology described in I. M. Alecu, J. Zheng, Y. Zhao, D. G. Truhlar, *J. Chem. Theory Comput.* 2010, **6**, 2872-2887.

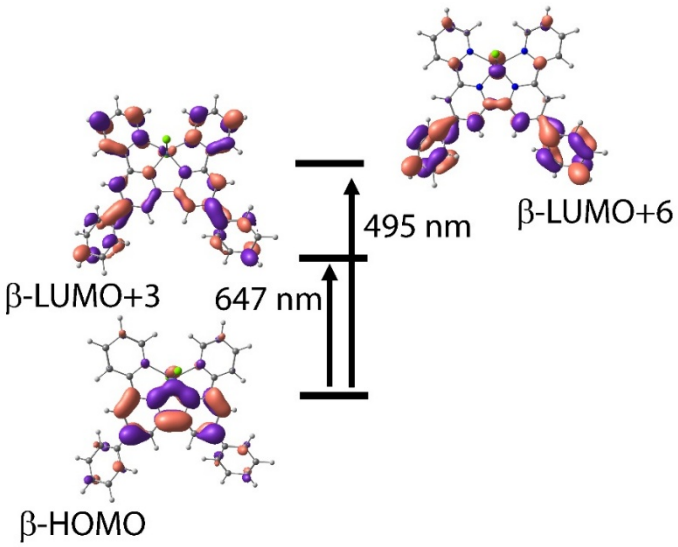

Figure S23. Selected transitions predicted by TD-DFT calculations (D3-B3LYP/6-31g*/PCM) for $[Cr(dpqpy)(Cl)_2]^0$

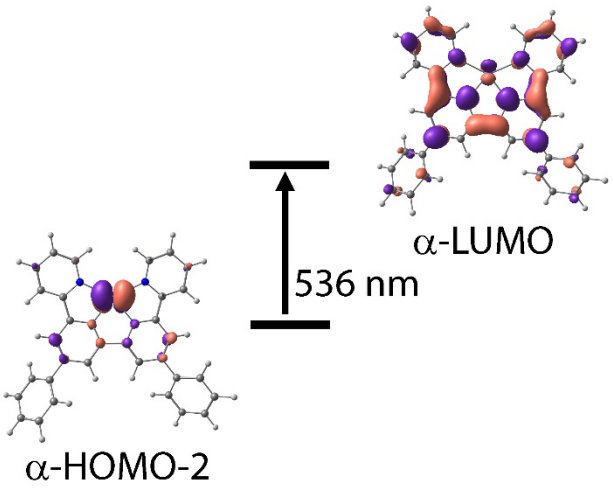

Figure S24. Selected transitions predicted by TD-DFT calculations (D3-B3LYP/6-31g*/PCM) for [Cr(d

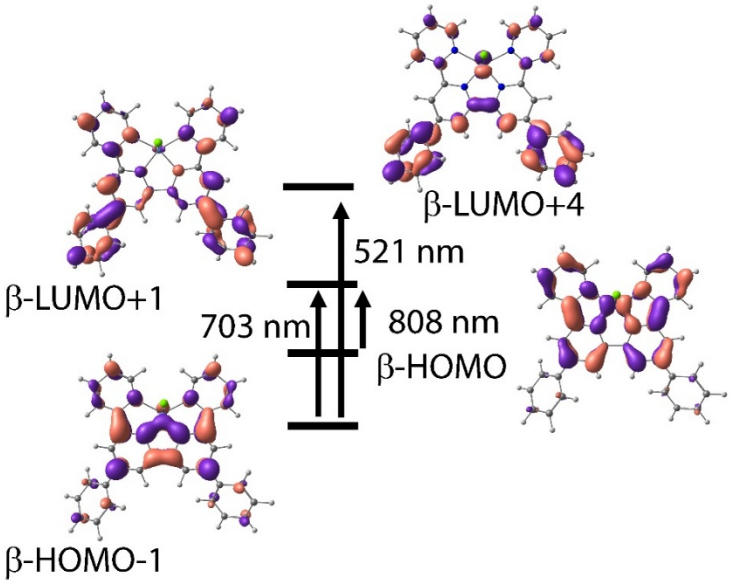

Figure S25. Selected transitions predicted by TD-DFT calculations (D3-B3LYP/6-31g*/PCM) for $[Cr(dpqpy)(Cl)_2]^+$

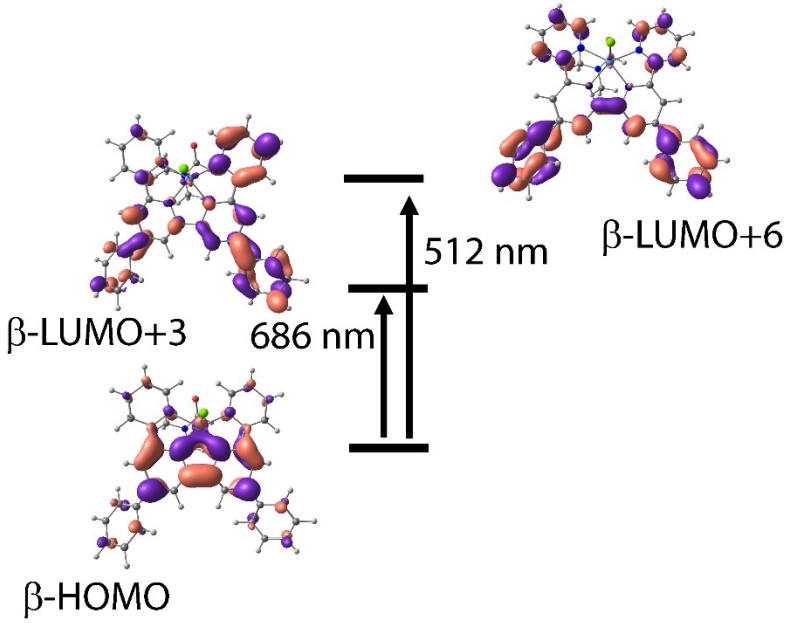

Figure S26. Selected transitions predicted by TD-DFT calculations (D3-B3LYP/6-31g*/PCM) for [Cr(dpqpy)(Cl)(DMF)]

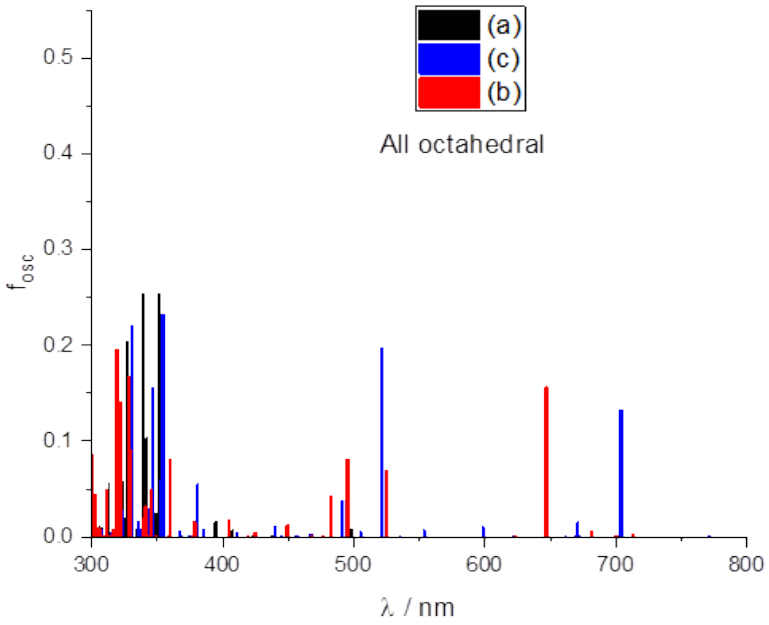

Figure S27. TD-DFT calculated electronic excitations of (a, black) $[Cr(dpqpy)(Cl)_2]^+$; (b, red) $[Cr(dpqpy)(Cl)_2]^0$; (c, blue) $[Cr(dpqpy)(Cl)_2]^-$). D3-B3LYP/6-31g*/PCM calculation.

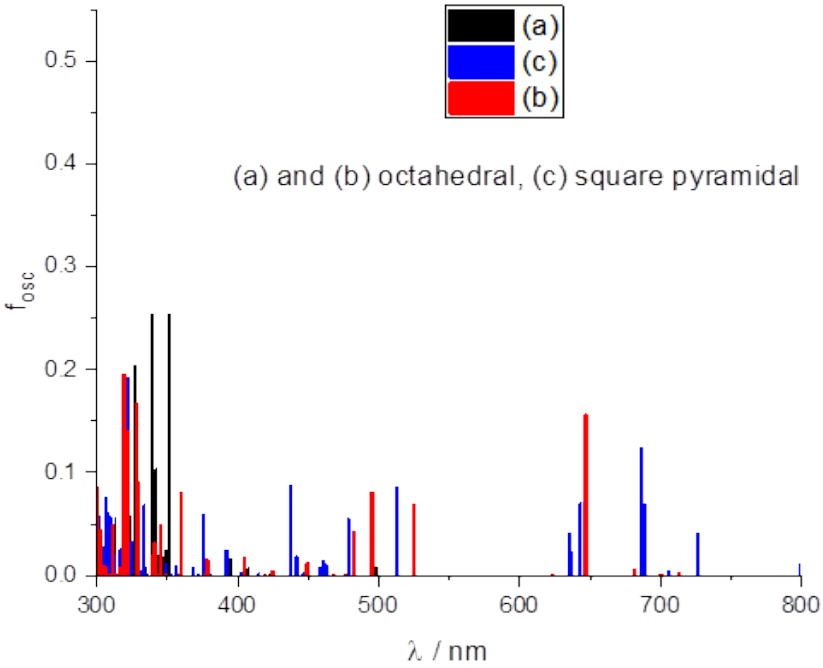

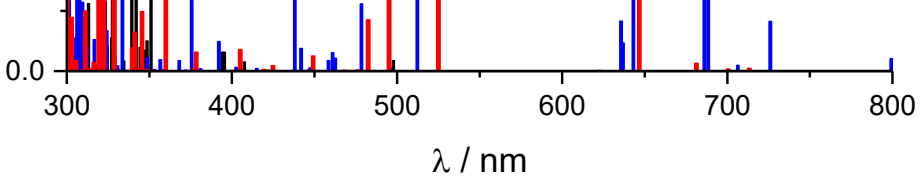

Figure S28. TD-DFT calculated electronic excitations of (a, black) $[Cr(dpqpy)(Cl)_2]^+$; (b, red) $[Cr(dpqpy)(Cl)_2]^0$; (c, blue) $[Cr(dpqpy)(Cl)]^+$, DMF. D3-B3LYP/6-31g*/PCM calculation.

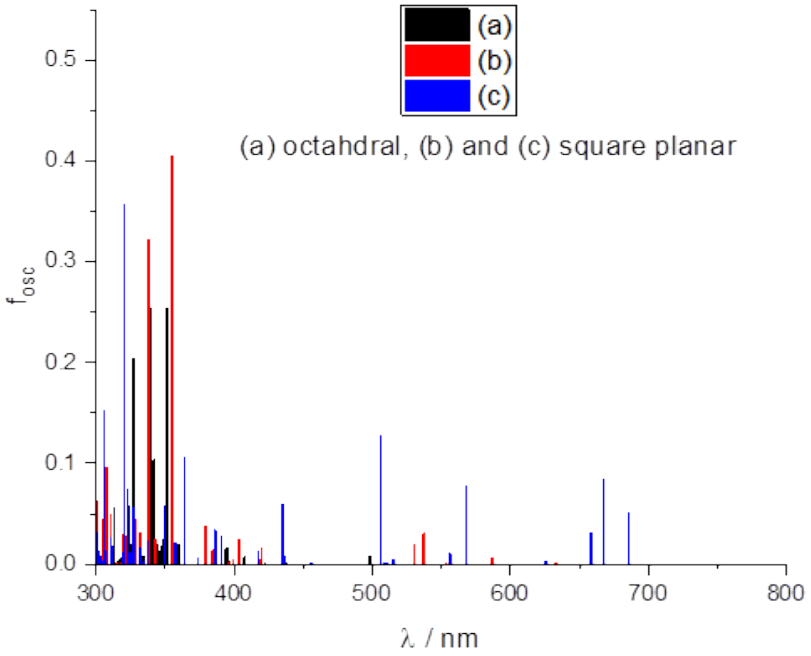

Figure S29. TD-DFT calculated electronic excitations of (a, black) $[Cr(dpqpy)(Cl)_2]^+$; (b, red) $[Cr(dpqpy)]^{2+}$; (c, blue) $[Cr(dpqpy)]^+$). D3-B3LYP/6-31g*/PCM calculation.

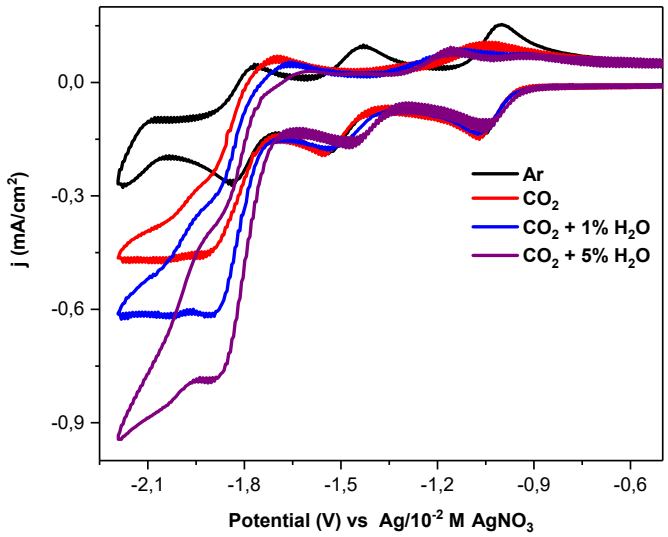

Figure S30. Cathodic CV scans of $[Cr(dpqpy)(Cl)_2]^+$ (1mM) in DMF/0.1M $TBAPF_6$ under argon (black), under CO_2 saturated conditions (red), under CO_2 saturated conditions and with

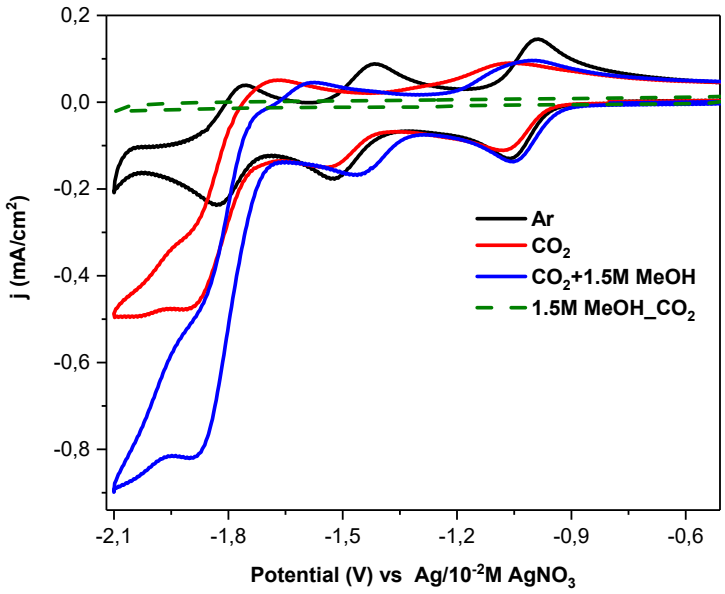

1%v/v H_2O (blue) and 5% v/v H_2O (purple) on GCE at $v = 0.1 Vs^{-1}$ electrode area 0.071 cm^2.

Figure S31. Cathodic CV scans in DMF/0.1M $TBAPF_6$ on GCE ($v = 0.1$ Vs^{-1}, electrode area 0.071 cm^2) of $[Cr(dpqpy)(Cl)_2]^+$ (1 mM) under argon (black), of $[Cr(dpqpy)(Cl)_2]^+$ (1 mM) under CO_2 saturated conditions (red), of $[Cr(dpqpy)(Cl)_2]^+$ (1 mM) under CO_2 saturated conditions with 1.5 M MeOH (blue), of MeOH (1.5 M) under CO_2 saturated condition (dotted line).

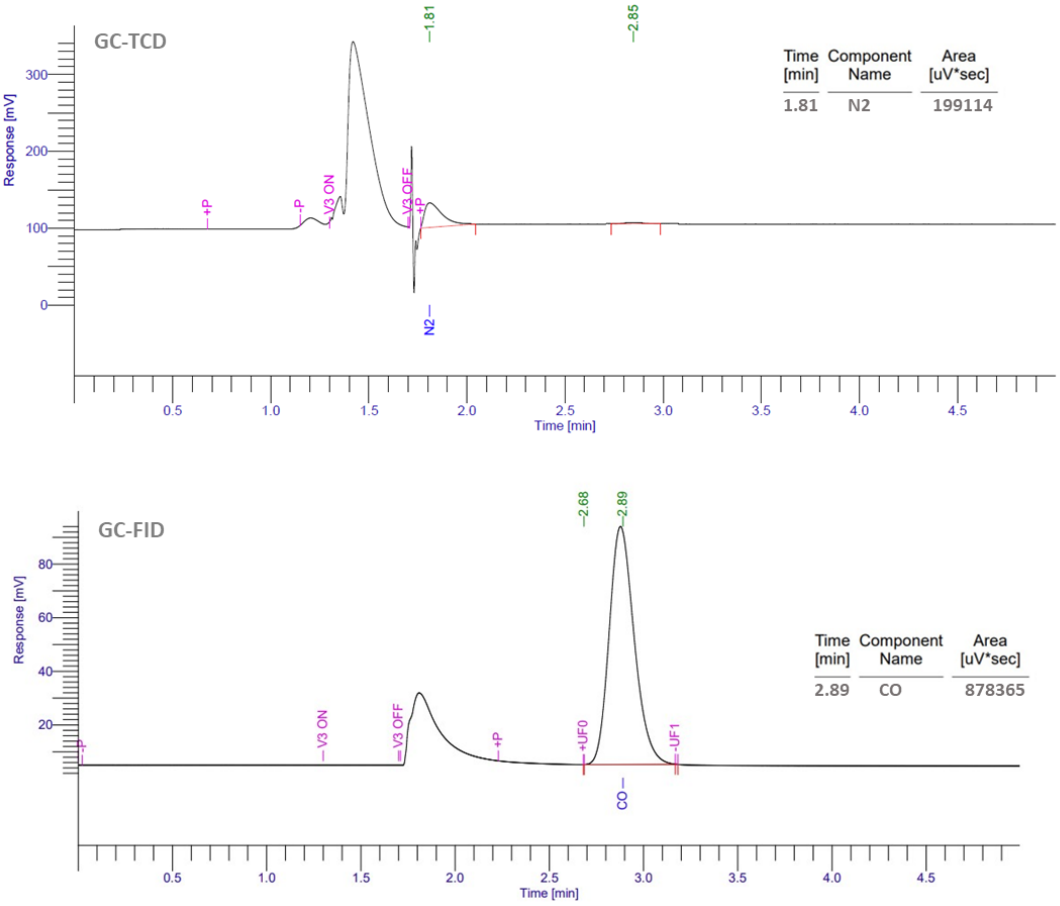

Figure S32. GC- Chromatogram recorded after 2h electrolysis performed at E = -1.85 V of $[Cr(dpqpy)(Cl)_2]^+$ (1mM) in DMF/0,1M $TBAPF_6$ under CO_2 saturated conditions in presence of PhOH 1.25 M. Above with a TCD (sensitive to H_2) and below a with FID (sensitive to CO) detection. (Q = -11.37 C).

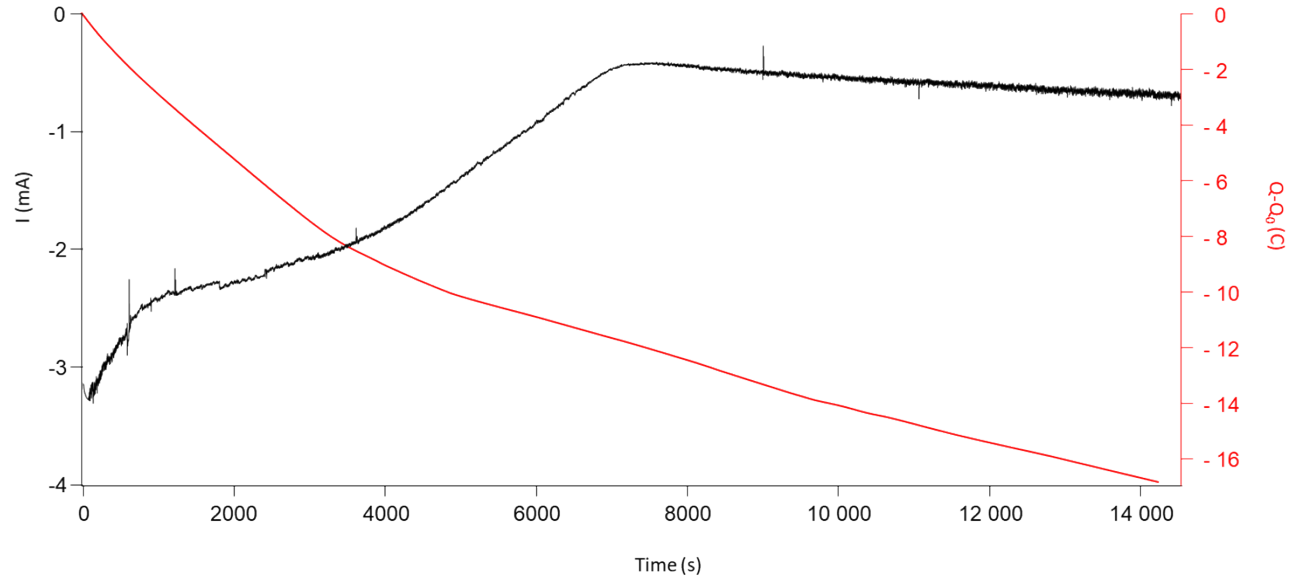

Figure S33. Chronoamperometry performed at E = -1.85 V of $[Cr(dpqpy)(Cl)_2]^+$ (1mM) in DMF/0.1M $TBAPF_6$ under CO_2 saturated conditions in presence of PhOH 1.25 M, working electrode: carbon foam 80 dpi (5 mm × 5 mm × 5 mm).

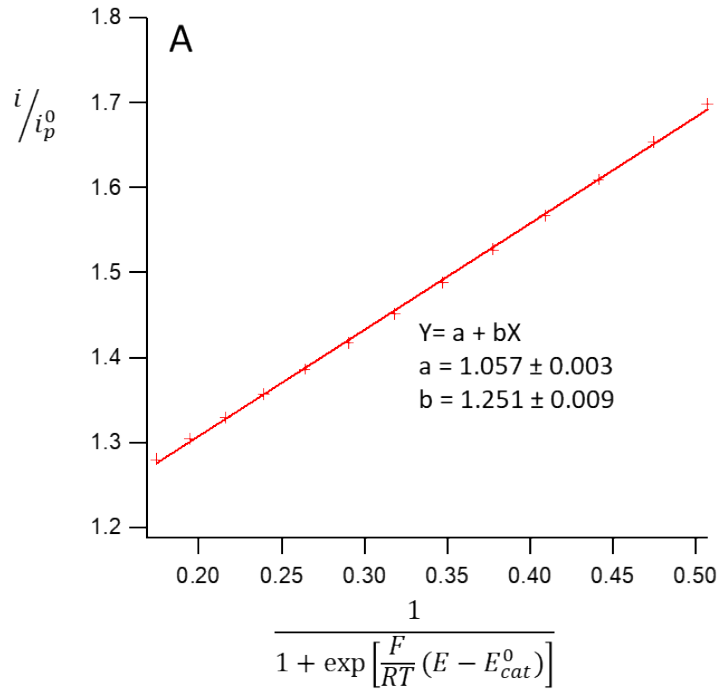

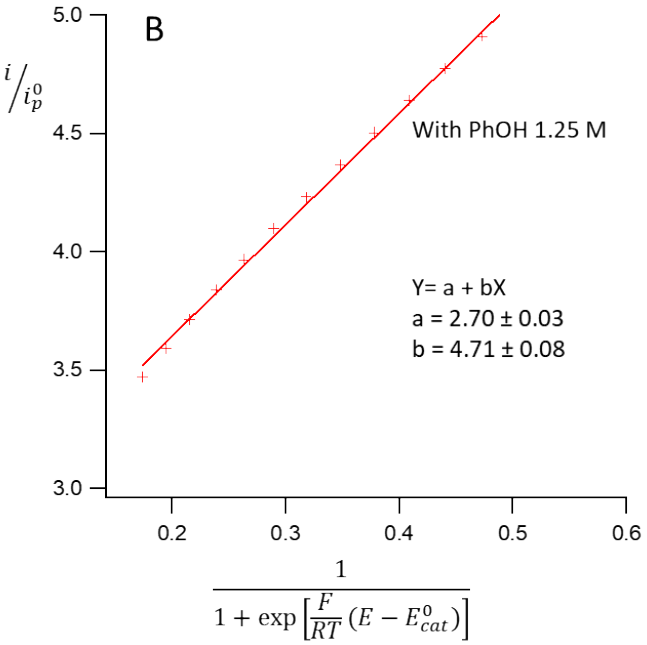

Figure S34. Foot of the wave analysis of the catalysis of CO_2 reduction by $[Cr(dpqpy)(Cl)_2]^+$ (1mM) in DMF/0.1 M $TBAPF_6$ under saturated CO_2 condition (A); and with 1.25 M PhOH (B)

2-Tables:

Table S1: Electronic structure of the free ligand and zinc complexes from DFT calculations[a]

Species	Spin state	Magnetic coupling [b]	$\Delta E_{(closed\ shell\ singlet\ -\ triplet)}$[c]
$(dpqpy^{2-})$	Closed-shell singlet	-	+6.8
$(dpqpy^{2\bullet 2-})$	Triplet	-	0
$(dpqpy^{2\bullet 2-})$	BS singlet	J = -43 cm^{-1}	-
$[Zn(dpqpy)(Cl)_2]^{2-}$	Closed-shell singlet	-	+2.7
	Triplet	-	0
	BS singlet	J = -425 cm^{-1}	-

[a] From a geometry optimization using the B3LYP functional (6-31g* basis set/PCM). All states were converged and frequency calculations confirm that they are real minimum and not saddle points. The bipyridine core is flat in the closed-shell singlet, but tilted in triplet $(dpqpy)^{2\bullet 2-}$ or umbrella-shaped in triplet $[Zn(dpqpy)(Cl)_2]^{2-}$. Within $[Zn(dpqpy)(Cl)_2]^{2-}$, the ligand is dianionic, either under a diradical form $(dpqpy)^{2\bullet 2-}$ or the closed-shell form $(dpqpy)^{2-}$.

[b] Calculated by using the Yamaguchi formula (T. Soda, Y. Kitagawa, T. Onishi, Y. Takano, Y. Shigeta, H. Nagao, Y. Yoshioka, K. Yamaguchi, *Chem. Phys. Lett.* **2000**, *319*, 223-230).

[c] in kcal/mol.

Table S2: Geometry and electronic structure of the complexes from DFT calculations with empirical dispersion [a]

Complex	Spin state	B3LYP[b]	D3-B3LYP[b]	D3-B3LYP[b] PCM	D3-B3LYP[c] PCM
$[Cr(dpqpy)(Cl)_2]^+$	**Quartet**	-	-	-	-
$[Cr(dpqpy)(Cl)_2]^0$	**BS triplet**	0	0	0	0 [d]
$[Cr(dpqpy)(Cl)_2]^0$	Quintet	+4.6	+4.6	+3.9	+3.7
$[Cr(dpqpy)(Cl)_2]^-$	**BS doublet**	0	0	0	0
$[Cr(dpqpy)(Cl)_2]^-$	Quartet	+6.5	+6.4	+5.1	+5.8
$[Cr(dpqpy)(Cl)_2]^-$	Sextet	+7.9	+7.7	+9.2	+9.9
$[Cr(dpqpy)(Cl)(DMF)]^0$	BS doublet	+5.7	+5.5	+3.3	+5.5
$[Cr(dpqpy)(Cl)]^0$, DMF	**BS quartet**	0	0	0	0 [d]
$[Cr(dpqpy)(Cl)(DMF)]^0$	Sextet	+13.6	+13.7	+13.7	+15.4
$[Cr(dpqpy)]^{2+}$	Triplet	+27.8	+87.0	+49.5	+35.0
$[Cr(dpqpy)]^{2+}$	**Quintet**	0	0	0	0
$[Cr(dpqpy)]^+$	BS doublet	+43.1	+42.9	+32.3	+31.4
$[Cr(dpqpy)]^+$	**BS quartet**	0	0	0	0
$[Cr(dpqpy)]^+$	Sextet	+0.5	+0.4	+2.1	+4.2

[a] From a geometry optimization using the B3LYP functional. All states were converged and frequency calculations confirm that they are real minima and not saddle points. Sum of electronic and thermal free energies, in kcal/mol. PCM indicates that a polarized continuum was used to model the solvent.

[b] 6-31g(d,p) basis set

[c] 6-311+G(2d,p) basis set

[d] Presence of one imaginary frequency > -100 cm^{-1} that cannot be removed, but which does not affect the nature of the ground spin state.

Table S3 : Mulliken spin populations on selected atoms of the ligand, from a B3LYP/6-31g* calculation[a]

Complex	Spin state	Cr	N1/N4	N2/N3	C1/C2	C3/C4	C5/C6	C7/C8	C9/C10
$[Cr(dpqpy)(Cl)_2]^+$	Quartet	3.03	-0.03	-0.05	0.02	0.02	0.02	0	0.02
$[Cr(dpqpy)(Cl)_2]^0$	BS triplet	2.96	-0.04	-0.22	-0.09	-0.12	-0.01	-0.02	0.05
$[Cr(dpqpy)(Cl)_2]^0$	Quintet	3.05	0	0.13	0.11	0.15	0.04	0.02	-0.06
$[Cr(dpqpy)(Cl)_2]^-$	BS doublet	2.94	-0.17	-0.25	0	-0.15	-0.12	-0.10	-0.07
$[Cr(dpqpy)(Cl)_2]^-$	quartet	2.97	0.02	-0.09	-0.06	-0.03	0.04	0	0.07
$[Cr(dpqpy)(Cl)_2]^-$	sextet	3.06	0.11	0.16	-0.03	0.12	0.16	0.05	0.16
$[Cr(dpqpy)(Cl)(DMF)]^0$	BS doublet	2.85	-0.15	-0.24	-0.02	-0.16	-0.14	-0.09	-0.04
$[Cr(dpqpy)(Cl)]^0$, DMF	BS quartet	3.53	-0.05	-0.18	-0.03	-0.06	0	-0.02	0.03
$[Cr(dpqpy)(Cl)(DMF)]^0$	sextet	3.12	0.11	0.14	0	0.14	0.19	0.14	0.11
$[Cr(dpqpy)]^{2+}$	BS triplet	1.85	-0.02	-0.03	0.03	0.03	0.03	0	0
$[Cr(dpqpy)]^{2+}$	Quintet	4.03	-0.05	-0.07	0.02	0.02	0.02	0	0
$[Cr(dpqpy)]^+$	BS doublet	1.86	-0.06	-0.14	0.09	-0.15	-0.08	-0.04	0.07
$[Cr(dpqpy)]^+$	quartet	3.96	-0.08	-0.20	-0.07	-0.13	-0.05	-0.03	0.06
$[Cr(dpqpy)]^+$	sextet	4.07	0	0.04	0.09	0.15	0.10	0.01	-0.06

[a] The atom numbering is depicted in the figure below:

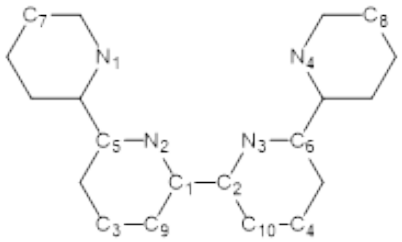

Table S4: Mulliken spin populations on selected atoms of the ligand, from a D3-B3LYP/6-31g* calculation[a]

Complex	Spin state	Cr	N1/N4	N2/N3	C1/C2	C3/C4	C5/C6	C7/C8	C9/C10
$[Cr(dpqpy)(Cl)_2]^+$	Quartet	3.03	-0.03	-0.05	0.02	0.02	0.02	0	0
$[Cr(dpqpy)(Cl)_2]^0$	BS triplet	2.96	-0.05	-0.22	-0.09	-0.12	-0.01	-0.2	0.05
$[Cr(dpqpy)(Cl)_2]^0$	Quintet	3.04	0	0.13	0.10	0.15	0.04	0.02	-0.06
$[Cr(dpqpy)(Cl)_2]^-$	BS doublet	2.94	-0.15	-0.27	0	-0.15	-0.12	-0.11	-0.08
$[Cr(dpqpy)(Cl)_2]^-$	quartet	2.97	0.03	-0.09	-0.06	-0.04	0.04	0.04	0.08
$[Cr(dpqpy)(Cl)_2]^-$	sextet	3.06	0.11	0.16	-0.03	0.12	0.17	0.16	0.16
$[Cr(dpqpy)(Cl)(DMF)]^0$	BS doublet	2.85	-0.15	-0.23	-0.02	-0.16	-0.14	-0.10	-0.03
$[Cr(dpqpy)(Cl)]^0$, DMF	BS quartet	3.67	-0.05	-0.21	-0.05	-0.08	0	-0.02	0.04
$[Cr(dpqpy)(Cl)(DMF)]^0$	sextet	3.09	0.11	0.14	0	0.14	0.19	0.15	0.11
$[Cr(dpqpy)]^{2+}$	BS triplet	1.87	-0.02	0.03	0	0	0	-0.01	0
$[Cr(dpqpy)]^{2+}$	Quintet	4.02	-0.07	-0.03	0.02	0	0	0	0.02
$[Cr(dpqpy)]^+$	BS doublet	1.85	-0.07	-0.14	-0.09	-0.15	-0.08	-0.04	0.07
$[Cr(dpqpy)]^+$	quartet	3.96	-0.08	-0.20	-0.07	-0.13	-0.05	-0.03	0.06
$[Cr(dpqpy)]^+$	sextet	4.07	0	0.04	0.09	0.15	0.10	0.01	-0.06

[a] The atom numbering is depicted in figure below:

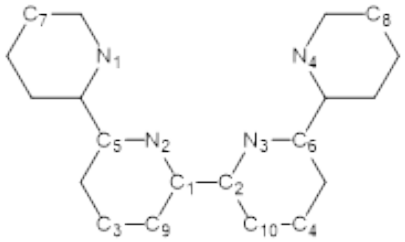

Table S5: Mulliken spin populations on selected atoms of the ligand, from a D3-B3LYP/6-31g*/PCM calculation[a]

Complex	Spin state	Cr	N1/N4	N2/N3	C1/C2	C3/C4	C5/C6	C7/C8	C9/C10
$[Cr(dpqpy)(Cl)_2]^+$	Quartet	3.07	-0.03	-0.05	0.02	0.02	0.2	0	0
$[Cr(dpqpy)(Cl)_2]^0$	BS triplet	2.97	-0.04	-0.21	-0.09	-0.12	-0.02	-0.02	0.05
$[Cr(dpqpy)(Cl)_2]^0$	Quintet	3.08	-0.01	0.12	0.12	0.14	0.03	0.01	-0.06
$[Cr(dpqpy)(Cl)_2]^-$	BS doublet	2.89	-0.15	-0.25	-0.02	-0.17	-0.14	-0.09	-0.04
$[Cr(dpqpy)(Cl)_2]^-$	quartet	2.96	0	-0.06	-0.04	0	0.03	0.02	0.02
$[Cr(dpqpy)(Cl)_2]^-$	sextet	3.09	0.12	0.14	-0.02	0.12	0.18	0.16	0.14
$[Cr(dpqpy)(Cl)(DMF)]^0$	BS doublet	2.83	-0.14	-0.24	-0.03	-0.17	-0.14	-0.08	-0.03
$[Cr(dpqpy)(Cl)]^0$, DMF	BS quartet	3.67	-0.05	-0.21	-0.05	-0.08	0	-0.02	0.04
$[Cr(dpqpy)(Cl)(DMF)]^0$	sextet	3.08	0.12	0.15	0	0.14	0.19	0.15	0.12
$[Cr(dpqpy)]^{2+}$	BS triplet	1.95	-0.02	-0.04	0.03	0.03	0.03	0	-0.01
$[Cr(dpqpy)]^{2+}$	Quintet	3.98	-0.03	-0.06	0.03	0.03	0.03	0	-0.01
$[Cr(dpqpy)]^+$	BS doublet	2.44	-0.09	-0.17	-0.08	-0.17	-0.12	-0.03	0.03
$[Cr(dpqpy)]^+$	quartet	3.94	-0.05	-0.22	-0.08	-0.12	-0.02	-0.02	0.06
$[Cr(dpqpy)]^+$	sextet	4.02	0	0.08	0.10	0.16	0.09	0.01	-0.06

[a] The atom numbering is depicted in figure below:

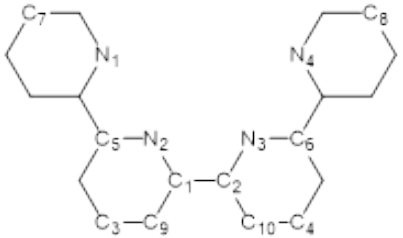

Table S6: Mulliken spin populations on selected atoms of the ligand, from a D3-B3LYP/6-311+G(2d,p)/PCM calculation[a]

Complex	Spin state	Cr	N1/N4	N2/N3	C1/C2	C3/C4	C5/C6	C7/C8	C9/C10
$[Cr(dpqpy)(Cl)_2]^+$	Quartet	3.45	-0.08	-0.12	-0.03	0.02	0	0.01	0
$[Cr(dpqpy)(Cl)_2]^0$	BS triplet	3.36	-0.09	-0.28	-0.14	-0.11	-0.04	-0.01	0.05
$[Cr(dpqpy)(Cl)_2]^0$	Quintet	3.44	-0.06	0.08	0.06	0.14	0	0.02	-0.04
$[Cr(dpqpy)(Cl)_2]^-$	BS doublet	3.25	-0.19	-0.31	-0.08	-0.16	-0.17	-0.09	-0.04
$[Cr(dpqpy)(Cl)_2]^-$	quartet	3.29	-0.05	-0.08	-0.06	0	-0.02	0.02	0.02
$[Cr(dpqpy)(Cl)_2]^-$	sextet	3.44	0.09	0.09	-0.05	0.11	0.14	0.19	0.15
$[Cr(dpqpy)(Cl)(DMF)]^0$	BS doublet	3.13	-0.18	-0.30	-0.08	-0.16	-0.16	-0.09	-0.02
$[Cr(dpqpy)(Cl)]^0$, DMF	BS quartet	3.29	-0.05	-0.08	-0.06	0	-0.02	0.02	0.02
$[Cr(dpqpy)(Cl)(DMF)]^0$	sextet	3.35	0.10	0.10	-0.04	0.13	0.16	0.18	-0.13
$[Cr(dpqpy)]^{2+}$	BS triplet	2.56	-0.05	-0.11	-0.07	-0.08	-0.04	-0.02	0.04
$[Cr(dpqpy)]^{2+}$	Quintet	4.01	-0.04	-0.09	0.02	0.03	0.04	0	-0.01
$[Cr(dpqpy)]^+$	BS doublet	2.40	-0.11	-0.10	-0.08	-0.15	-0.09	-0.04	0.03
$[Cr(dpqpy)]^+$	quartet	3.99	-0.07	-0.26	-0.08	-0.10	0	-0.02	0.05
$[Cr(dpqpy)]^+$	sextet	4.04	0	0.09	0.09	0.15	0.08	0.03	-0.05

[a] The atom numbering is depicted in figure below:

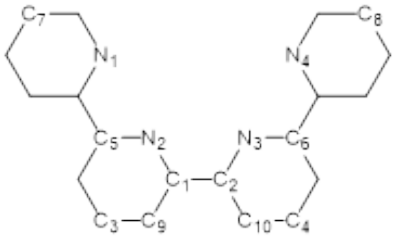

Table S7: Calculation of CO production (n CO) and faradaic efficiency (F.E.) for the electrocatalytic reduction of CO_2 at E=-1.85 V by $[Cr(dpqpy)(Cl)_2]^+$ (1mM) in DMF/0.1 M $TBAPF_6$ + 1.0 M PhOH.

Calibration curve : Area $_{CO}$ = $1.46791 \times 10^8 T_{CO}$ and $n_{CO} = (T_{CO} \times 140 \times 10^{-3})/ 22.4$

Time (min.)	Q (C.)	Peak CO area	n CO (mol.)	F.E. (%)
0		371	1.58×10^{-8}	
30	- 4.41	85358	3.63×10^{-6}	16
60	- 8.35	245366	1.04×10^{-5}	24
90	- 11.06	310774	1.32×10^{-5}	23
120	- 12.85	282937	1.20×10^{-5}	18
150	- 15.05	306360	1.30×10^{-5}	17
180	- 17.08	296792	1.26×10^{-5}	14
210	- 18.49	274856	1.17×10^{-5}	12
240	- 19.61	272582	1.16×10^{-5}	11

Table S8: Calculation of CO production (n CO) and faradaic efficiency (F.E.) for the electrocatalytic reduction of CO_2 at E=-1.85 V by $[Cr(dpqpy)(Cl)_2]^+$ (1mM) in DMF/0.1 M $TBAPF_6$ + 1.25 M PhOH.

Calibration curve : Area $_{CO}$ = $1.5552 \times 10^8 T_{CO}$ and $n_{CO} = (T_{CO} \times 140 \times 10^{-3})/ 22.4$

Time (min.)	Q (C)	Peak CO area	n CO (mol)	F.E. (%)
0		152	6.10×10^{-9}	
30	- 4.66	174674	7.02×10^{-6}	29
60	- 8.53	521787	2.10×10^{-5}	48
90	- 10.53	763125	3.07×10^{-5}	56
120	- 11.37	878365	3.53×10^{-5}	60
150	- 13.60	789651	3.17×10^{-5}	45
180	- 14.70	725268	2.91×10^{-5}	38
210	- 15.70	680303	2.73×10^{-5}	34
240	- 16.86	664672	2.67×10^{-5}	31

Table S9: Calculation of CO production (n CO) and faradaic efficiency (F.E.) for the electrocatalytic reduction of CO_2 at E=-1.85 V by $[Cr(dpqpy)(Cl)_2]^+$ (1mM) in DMF/0.1 M $TBAPF_6$ + 1.5 M PhOH

Calibration curve : Area CO = $1.54284 \times 10^8 T_{CO}$ and $n_{CO} = (T_{CO} \times 140 \times 10^{-3})/ 22.4$

Time (min.)	Q (C.)	Peak CO area	n CO (mol.)	F.E. (%)
0		768	3.11×10^{-8}	
30	- 3.96	129127	6.74×10^{-6}	25
60	- 7.64	486353	1.97×10^{-5}	49
90	- 9.87	646859	2.62×10^{-5}	51
120	-10.02	703575	2.85×10^{-5}	55
150	-13.27	627080	2.54×10^{-5}	37
180	-15.46	619745	2.51×10^{-5}	31
210	-16.96	613199	2.48×10^{-5}	28
240	-19.21	573802	2.32×10^{-5}	23

Table S10: Calculation of CO production (n CO) and faradaic efficiency (F.E.) for the electrocatalytic reduction of CO_2 at E=-1.85 V by $[Cr(dpqpy)(Cl)_2]^+$ (1mM) in DMF/0.1 M $TBAPF_6$ + 1.75 M PhOH

Calibration curve : Area CO = $1.46791 \times 10^8 T_{CO}$ and $n_{CO} = (T_{CO} \times 140 \times 10^{-3})/ 22.4$

Time (min.)	Q (C.)	Peak CO area	n CO (mol.)	F.E. (%)
0		523	2.23×10^{-8}	
30	- 4.18	82368	3.51×10^{-6}	16
60	- 6.20	233625	9.94×10^{-6}	30
90	- 9.32	378127	1.61×10^{-5}	33
120	- 11.21	478458	2.04×10^{-5}	35
150	- 11.41	442135	1.88×10^{-5}	32
180	- 14.32	426653	1.82×10^{-5}	24
210	- 16.49	423752	1.80×10^{-5}	21
240	- 19.68	414757	1.77×10^{-5}	17